JCI The Journal of Clinical Investigation

Cycling CD4+ T cells in HIV-infected immune nonresponders have mitochondrial dysfunction

Souheil-Antoine Younes, … , Benigno Rodriguez, Michael M. Lederman

J Clin Invest. 2018;128(11):5083-5094. https://doi.org/10.1172/JCI120245.

Research Article AIDS/HIV Metabolism

Immune nonresponder (INR) HIV-1–infected subjects are characterized by their inability to reconstitute the CD4+ T cell pool after antiretroviral therapy. This is linked to poor clinical outcome. Mechanisms underlying immune reconstitution failure are poorly understood, although, counterintuitively, INRs often have increased frequencies of circulating CD4+ T cells in the cell cycle. While cycling CD4+ T cells from healthy controls and HIV+ patients with restored CD4+ T cell numbers complete cell division in vitro, cycling CD4+ T cells from INRs do not. Here, we show that cells with the phenotype and transcriptional profile of Tregs were enriched among cycling cells in health and in HIV infection. Yet there were diminished frequencies and numbers of Tregs among cycling CD4+ T cells in INRs, and cycling CD4+ T cells from INR subjects displayed transcriptional profiles associated with the impaired development and maintenance of functional Tregs. Flow cytometric assessment of TGF-β activity confirmed the dysfunction of Tregs in INR subjects. Transcriptional profiling and flow cytometry revealed diminished mitochondrial fitness in Tregs among INRs, and cycling Tregs from INRs had low expression of the mitochondrial biogenesis regulators peroxisome proliferator–activated receptor γ coactivator 1-α (PGC1α) and transcription factor A for mitochondria (TFAM). In vitro exposure to IL-15 allowed cells to complete division, restored the expression of PGC1α and TFAM, and regenerated mitochondrial fitness in the cycling […]

Cycling CD4+ T cells in HIV-infected immune nonresponders have mitochondrial dysfunction

Souheil-Antoine Younes,[1] Aarthi Talla,[2] Susan Pereira Ribeiro,[2] Evgeniya V. Saidakova,[3] Larisa B. Korolevskaya,[3] Konstantin V. Shmagel,[3] Carey L. Shive,[1,4] Michael L. Freeman,[1] Soumya Panigrahi,[1] Sophia Zweig,[1] Robert Balderas,[5] Leonid Margolis,[6] Daniel C. Douek,[7] Donald D. Anthony,[1,4] Pushpa Pandiyan,[8] Mark Cameron,[2] Scott F. Sieg,[1] Leonard H. Calabrese,[9] Benigno Rodriguez,[1] and Michael M. Lederman[1]

[1]Division of Infectious Disease and [2]Department of Pathology, Case Western Reserve University, Cleveland, Ohio, USA. [3]Institute of Ecology and Genetics of Microorganisms, Perm, Russia. [4]Divisions of Infectious and Rheumatic Diseases, University Hospitals Case Medical Center, The Cleveland VA Medical Center, and the Center for AIDS Research, Cleveland, Ohio, USA. [5]Becton Dickinson, San Diego, California, USA. [6]National Institute of Child Health and Human Development and [7]Human Immunology Section, Vaccine Research Center, National Institutes of Allergy and Infectious Diseases (NIAID), NIH, Bethesda, Maryland, USA. [8]School of Dental Medicine, Case Western Reserve University, Cleveland, Ohio, USA. [9]Rheumatologic and Immunologic Disease, Cleveland Clinic, Cleveland, Ohio, USA.

Immune nonresponder (INR) HIV-1–infected subjects are characterized by their inability to reconstitute the CD4+ T cell pool after antiretroviral therapy. This is linked to poor clinical outcome. Mechanisms underlying immune reconstitution failure are poorly understood, although, counterintuitively, INRs often have increased frequencies of circulating CD4+ T cells in the cell cycle. While cycling CD4+ T cells from healthy controls and HIV+ patients with restored CD4+ T cell numbers complete cell division in vitro, cycling CD4+ T cells from INRs do not. Here, we show that cells with the phenotype and transcriptional profile of Tregs were enriched among cycling cells in health and in HIV infection. Yet there were diminished frequencies and numbers of Tregs among cycling CD4+ T cells in INRs, and cycling CD4+ T cells from INR subjects displayed transcriptional profiles associated with the impaired development and maintenance of functional Tregs. Flow cytometric assessment of TGF-β activity confirmed the dysfunction of Tregs in INR subjects. Transcriptional profiling and flow cytometry revealed diminished mitochondrial fitness in Tregs among INRs, and cycling Tregs from INRs had low expression of the mitochondrial biogenesis regulators peroxisome proliferator–activated receptor γ coactivator 1-α (PGC1α) and transcription factor A for mitochondria (TFAM). In vitro exposure to IL-15 allowed cells to complete division, restored the expression of PGC1α and TFAM, and regenerated mitochondrial fitness in the cycling Tregs of INRs. Our data suggest that rescuing mitochondrial function could correct the immune dysfunction characteristic of Tregs in HIV-1–infected subjects who fail to restore CD4+ T cells during antiretroviral therapy.

Introduction

The introduction of combination antiretroviral therapy (cART) has had a major impact on the morbidity and mortality of HIV-1–infected individuals. Nonetheless, despite effective control of HIV replication with cART, a minority of treated individuals fails to show increased CD4+ T cell counts to the levels observed in uninfected subjects (1, 2). These immune failure or immune nonresponder (INR) subjects remain at greater risk for morbidity and mortality than do immune responder (IR) subjects in whom the CD4+ T cell count is restored (3, 4). Although the precise determinants of immune failure are not well defined, several characteristics of immune cells define this syndrome and may provide insight into these mechanisms. High levels of T cell activation and cycling have been observed in many lymphopenic systems (5). INRs have high levels of T cell activation, defined by the coexpression of CD38 and HLA-DR on CD4+ and CD8+ T cells, as well as elevated expression of inflammatory markers in plasma (1). INRs also have profound decreases in circulating naive CD4+ and CD8+ T cells (1, 6, 7), and their lymphocytes have poor in vitro responses to IL-7 (8–11). Age (12, 3), nadir CD4+ T cell counts (14, 15), longer duration of HIV-1 infection (12, 3), microbial translocation and inflammation (1), and poor responses to IL-7 (8–11) have all been associated with the failure to restore CD4+ T cell numbers in INR subjects. Hepatitis C virus (HCV) coinfection has also been linked to low CD4+ T cell counts in some (16) but not all studies (17). Despite low CD4+ T cell numbers and poor IL-7 responsiveness, an increased frequency of cycling CD4+ T cells is characteristic of INRs (1, 2).

To better understand the characteristics of cycling CD4+ T cells in INRs, we used surface CD71 as a specific marker of cells in cycle and examined the transcriptional profile of cycling and noncycling memory CD4+ T cells from INRs, IRs, and healthy controls (HCs). We found that in each subject population, cycling CD4+ T cells were enriched for cells with the transcriptional profile and phenotype of Tregs, and we detected an apoptotic gene signature in cycling CD4+ T cells from INRs, but not in cycling cells from HCs or IRs. We also found that the impaired Treg homeostasis was linked to decreased CD4+ T cell counts in treated HIV

Authorship note: SAY, AT, and SPR contributed equally to this work.
Conflict of interest: The authors have declared that no conflict of interest exists.

Submitted: January 29, 2018; **Accepted:** September 4, 2018.
Reference information: *J Clin Invest*. 2018;128(11):5083–5094.
https://doi.org/10.1172/JCI120245.

infection. Mitochondria are the energy powerhouse organelles, and their function is linked to cell survival and function (18–20). Importantly, cycling Tregs from INR subjects showed decreased mitochondrial fitness and low expression of mitochondrial biogenesis regulators, the peroxisome proliferator–activated receptor γ coactivator 1-α (PGC1α), and the transcription factor A for mitochondria (TFAM). PGC1α is downregulated in settings of immune exhaustion such as that seen in murine lymphocytic choriomeningitis virus (LCMV) infection and in cancer models (21, 22). We found that in vitro exposure to IL-15 restored the expression of PGC1α and TFAM and regenerated mitochondrial fitness in cycling Tregs from INRs. We propose a model in which INR subjects fail to restore $CD4^+$ T cells as a consequence of defective Treg survival and function, resulting in a phenotype of uncontrolled cycling, immune exhaustion, and increased cell death.

Results

Tregs are enriched in cycling memory $CD4^+$ T cells, yet their frequency is diminished in INRs. To identify the mechanism that drives $CD4^+$ T cell cycling in cART-treated subjects, we sorted memory $CD4^+$ T cells expressing the transferrin receptor CD71. CD71 was recently identified as a surrogate for Ki67 in both human $CD8^+$ T cells (23) and mouse T cells (24). Here, we expand these findings to human $CD4^+$ T cells, as we observed that cell-surface expression of CD71 was tightly correlated to intracellular expression of Ki67 (r = 0.9854) among $CD4^+$ T cells (Supplemental Figure 1, A and B; supplemental material available online with this article; https://doi.org/10.1172/JCI120245DS1). We found that the frequency of cycling memory $CD4^+$ T cells as identified by Ki67 expression (Figure 1A) in subjects from a Russian cohort (n = 20 HCs, n = 21 IRs, and n = 16 INRs; Supplemental Table 1), or by CD71 expression (Figure 1B) in subjects from a Cleveland cohort (n = 10 HCs, n = 20 IRs, and n = 16 INRs; Supplemental Table 3) was increased in INRs compared with cycling frequencies in the IRs or HCs, confirming previous observations (1, 2). We applied the same criteria for INRs as in our earlier description of INRs (1). INRs were defined as having $CD4^+$ T cell counts below 350 cells/μl and IRs as having $CD4^+$ T cells counts above 350/μl after at least 2 years of cART with virologic control. Microarray analysis of sorted $CD71^+CD45RA^-CD4^+$ T cells (cycling memory cells) and $CD71^-CD45RA^-CD4^+$ T cells (noncycling memory cells) from 6 HCs, 6 IRs, and 6 INRs (Supplemental Table 2) confirmed that $CD71^+$ cells in all 3 groups upregulated cell-cycle–related gene modules (e.g., CDK1, CDK4, CDC20) (Figure 1C, Supplemental Figure 1C, and Supplemental Table 4) and downregulated genes that inhibit cell-cycle entry (e.g., CDKN2A, CDKN2B, CDKN1C) (Supplemental Figure 1D and Supplemental Table 4), thus validating the use of surface CD71 expression to identify $CD4^+$ T cells in cell cycle.

We also found significantly higher frequencies ($P < 0.05$) of phenotypically defined Tregs ($FOXP3^+CD127^-CD25^+$) among cycling memory cells (Supplemental Figure 2A) than among noncycling memory $CD4^+$ T cells in all 3 subject groups (Supplemental Figure 2B). Transcriptional profiling showed that genes typically expressed by Tregs (CTLA-4, IL-2RA [also known as CD25], ICOS) were upregulated in cycling memory cells when compared with their expression in noncycling memory cells in all 3 subject groups (Figure 1D), confirming the flow cytometric phenotypes shown in Supplemental Figure 2B. Nonetheless, Treg frequencies were significantly diminished among cycling memory cells of INRs compared with their frequencies among cycling memory cells of IRs (Figure 2A), and the frequencies of Tregs among cycling memory cells were inversely correlated with cycling frequencies ($CD71^+$) among total $CD4^+$ T cells (Figure 2B). Finally, the proportion of Tregs among cycling memory $CD4^+$ T cells and the peripheral $CD4^+$ T cell count (in IRs and INRs) were positively correlated in the HIV^+ subjects (Figure 2C).

Although the frequencies of cycling $CD4^+$ T cells were elevated in INRs compared with frequencies in IRs, the absolute numbers of both cycling and noncycling Tregs in circulation remained significantly lower in INRs than in IRs (Supplemental Figure 2C). These data suggest a potentially important role of Tregs in the homeostatic maintenance of $CD4^+$ T cell numbers (25).

The expression of genes that regulate Treg differentiation and function is suppressed in INRs. We then fit a linear model between Treg frequencies and gene expression pathways specific to Treg function (Supplemental Table 5). We found that the expression of genes specific to Treg function was associated with higher Treg frequencies in cycling memory $CD4^+$ T cells (normalized enrichment score [NES] = 1.6, $P < 0.05$) (Figure 3A). The expression of genes upregulated by the master transcription factor of Treg differentiation and function FOXP3 (26) (i.e., CD2, TNFRSF4, CD83) was linked to increased frequencies of cycling effector Tregs and was lower in INRs (NES = 1.9, $P < 0.05$) (Figure 3B). These findings were extended to a signature that includes genes of the TGF-β signaling pathway (TGIF1, SMAD1, SMAD7, LEFTY) (Figure 3C). TGF-β controls the development, differentiation, and function of Tregs (27) (NES = 1.7, $P < 0.05$), which further validates our model.

Deletion of Tregs can lead to systemic inflammation (28, 29), confirming their role in controlling inflammatory processes driven by type I IFNs (30, 31). IFN-stimulated genes (ISGs) were upregulated in INRs, and overall, this was inversely associated with Treg frequencies in cycling memory $CD4^+$ T cells (NES = –1.4, $P < 0.05$) (Figure 3D).

To further explore Treg function in phenotypically defined Tregs among INRs, we measured the expression of glycoprotein A repetitions predominant (GARP) and latency-associated peptide (LAP) as surrogates of TGF-β secretion (32). As shown in Figure 3F (and Supplemental Figure 3), the frequencies and absolute numbers (Supplemental Figure 3B) of cells expressing GARP and LAP among Tregs were significantly lower ($P < 0.05$) in INRs than in IRs, reflecting a diminished production of TGF-β by INR Tregs. Moreover, we established significant positive correlations between the numbers of peripheral $CD4^+$ T cells and the frequencies of phenotypically defined Tregs expressing GARP and LAP in treated HIV infection (IRs plus INRs) ($P = 0.02$, rho = 0.4) (Figure 3G). Taken together, these data suggest that Treg production of TGF-β is impaired in the setting of immune nonresponse and suggest that Treg dysfunction may underlie $CD4^+$ T cell homeostatic failure in treated HIV infection or is a consequence of it.

To explore the potential mechanisms for Treg dysfunction, we examined the oxidative phosphorylation (OXPHOS) pathway, which is associated with the development and maintenance of Tregs (33, 34). We found that expression of OXPHOS genes was positively correlated with the increasing frequency of Tregs in cycling memory $CD4^+$ T cells (NES = 2.1, $P < 0.0001$) (Figure 3E).

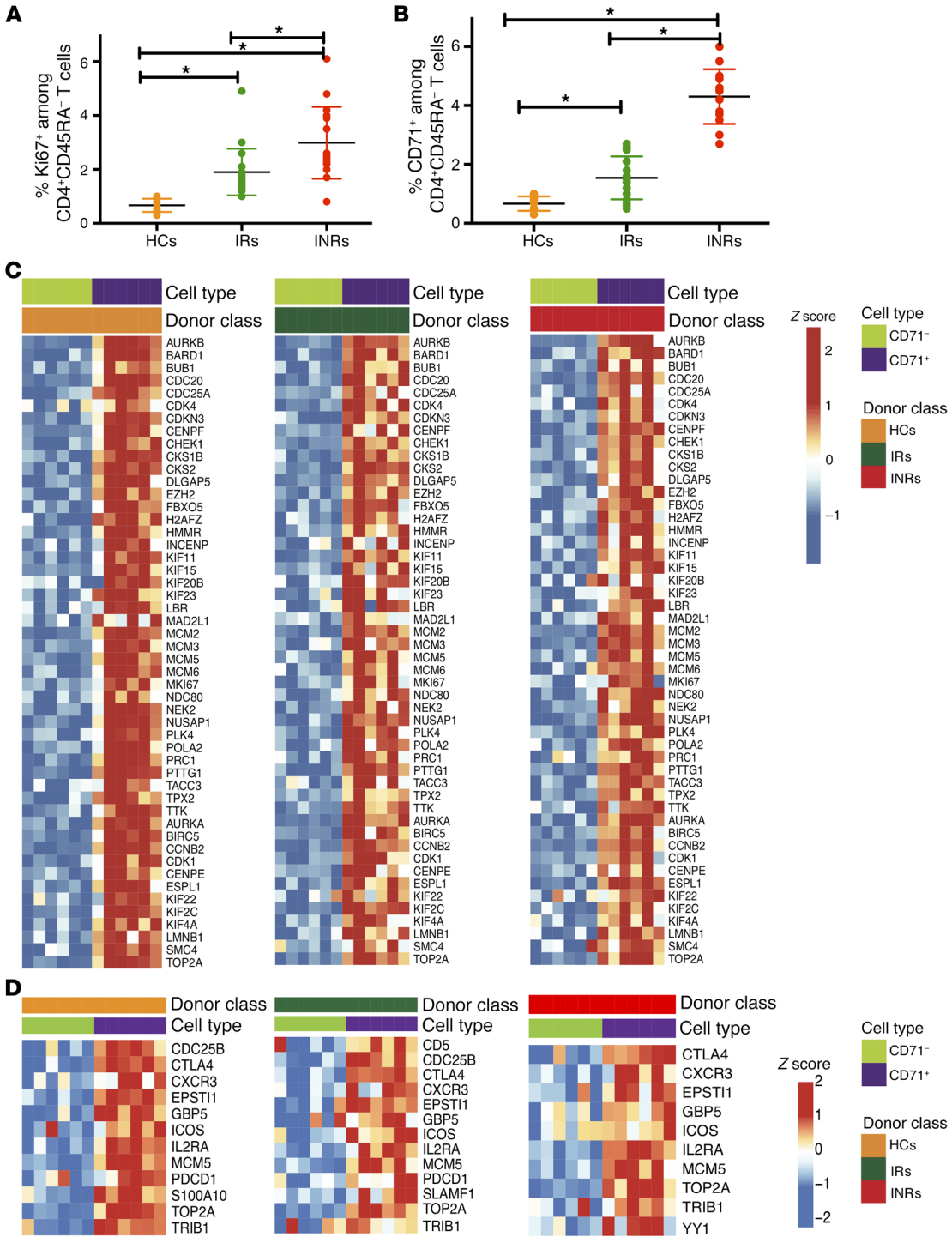

Figure 1. Cycling memory CD4⁺ T cells are enriched in Tregs. Frequency of cycling CD4⁺CD45RA⁻ T cells detected by (**A**) Ki67 expression in HCs (n = 20), IRs (n =21), and INRs (n = 16) or by (**B**) CD71⁺ expression in HCs (n = 10), IRs (n = 20), and INRs (n = 16) among subjects from the Russian cohort (**A**) and the Cleveland cohort (**B**) (*P < 0.05). (**C**) Heatmaps of cell-cycling–related modules comparing cycling and noncycling memory cells (P < 0.05) from HCs, IRs, and INRs of the Russian cohort. (**D**) Heatmaps of the Treg signatures showing upregulation (P < 0.05) in the cycling memory (CD45RA⁻CD71⁺) CD4⁺ T cells compared with signatures in noncycling memory (CD45RA⁻CD71⁻) CD4⁺ T cells from HCs (n = 6), IRs (n = 6), and INRs (n = 6) of the Russian cohort. P values for **A** and **B** were determined by a Wilcoxon rank-sum test. Data represent the mean ± SD.

Cycling CD4⁺ T cells from INRs have distinct gene expression profiles reflecting apoptotic signaling and inflammatory responses. Having demonstrated that Treg dysfunction is characteristic of cycling CD4⁺ T cells in INRs, we next explored potential mechanisms that could explain the low CD4⁺ T cell numbers observed in INRs. We monitored for differences in gene expression profiles of the cycling memory cells among the 3 groups and found that the gene expression profiles of the HCs and IRs were similar and dis-

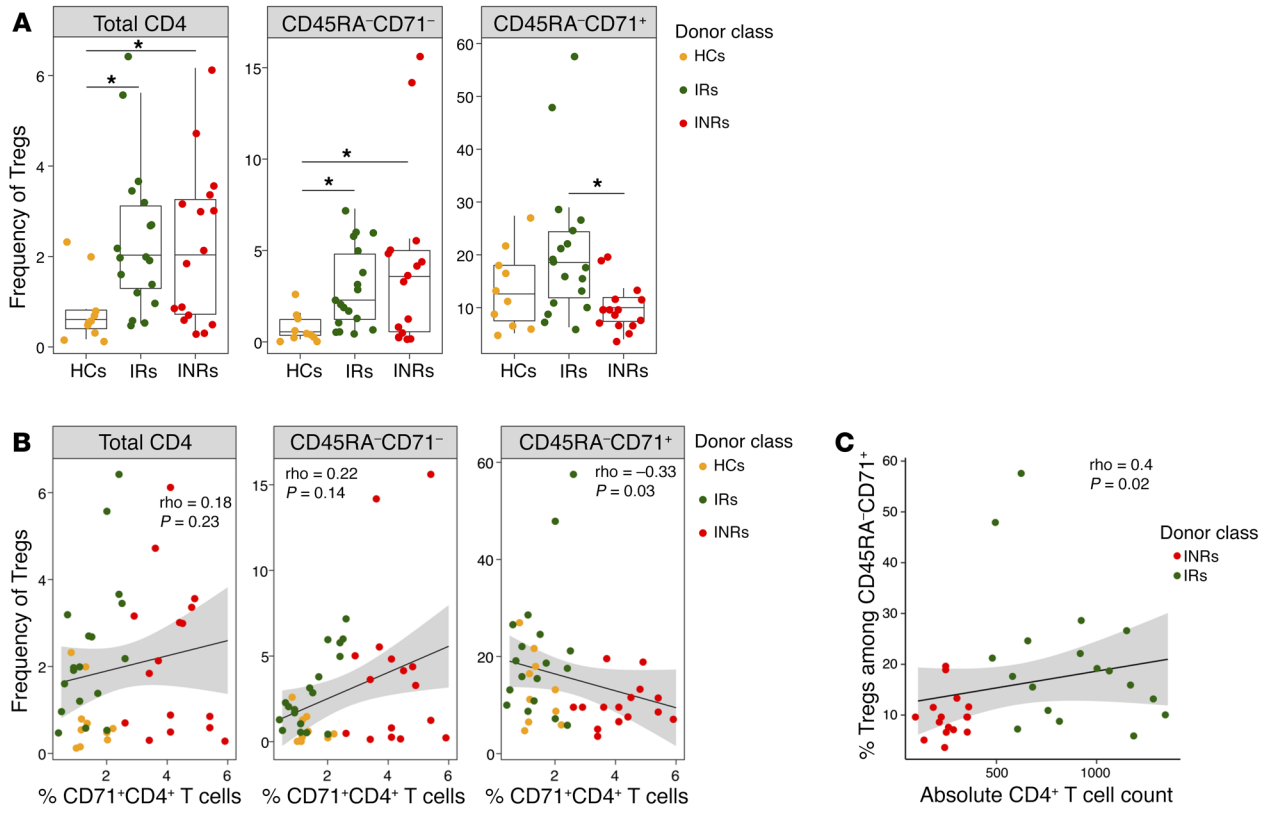

Figure 2. Cycling Tregs are linked to CD4⁺T cell homeostasis. (**A**) Proportions of Tregs (FOXP3⁺CD25⁺CD127⁻) among all CD4⁺ T cells among noncycling memory (CD71⁻CD45RA⁻) CD4⁺ T cells and cycling (CD71⁺) memory CD4⁺ T cells (n = 46, Cleveland cohort subjects) (*P < 0.05). (**B**) Spearman's correlation between Treg frequencies (y axis) in CD4⁺ T cells in noncycling memory and cycling memory CD4⁺ T cells with the frequencies of CD71⁺ cells among CD4⁺ T cells (x axis) (n = 46, Cleveland cohort subjects). (**C**) Spearman's correlation between the frequency of Tregs among cycling memory CD4⁺ T cells and the absolute CD4⁺ T cell count in HIV⁺ donors (n = 36, Cleveland cohort subjects). P values for **A** were determined by a Wilcoxon rank-sum test. Data represent the mean ± SD.

tinct from those of the INR subjects (Supplemental Figure 4A and Supplemental Table 6). We then used the gap statistic approach (35) to identify the genes that showed distinct expression profiles among these groups and characterized pathways enriched among the genes (see Methods). This analysis revealed that the expression of proapoptotic genes in cycling CD4⁺ T cells was significantly (P < 0.05) upregulated specifically in the INRs when compared with expression of these genes in IRs and HCs (Figure 4A). Type I IFN triggers the expression of several proapoptotic genes (36). Figure 4B shows that ISGs, including proapoptotic genes (IFI27, IFIT2, SAMD9), were significantly upregulated in cycling CD4⁺ T cells from INRs. As expected, higher expression of these ISGs was associated with lower absolute numbers of CD4⁺ T cells and, importantly, with lower frequencies of phenotypically defined Tregs among cycling memory CD4⁺ T cells (Supplemental Figure 4, B and C, and Figure 4, C and D). These 2 pathways (type I IFN and apoptosis) were also positively correlated with the frequency of cycling (Ki67⁺) CD4⁺ T cells, a hallmark feature of disrupted T cell homeostasis among INRs (Supplemental Figure 4, D and E). These signatures, which were observed to be specific to the cycling memory cells of INRs, were not observed in their noncycling memory cell counterparts (data not shown).

These apoptotic gene signatures were relevant to cell survival, as in short-term culture experiments (Figure 4, E and F) we found that sorted (CD71⁺) cycling cells from INRs failed to complete the cell cycle and divide ex vivo, and this was associated with a profound loss of viability that we did not observe in the cycling or noncycling cells from IRs or HCs or among the noncycling cells from INRs (Figure 4G).

OXPHOS and mitochondrial mass are downregulated in the cycling Tregs of INRs. As mitochondrial function is linked to cell survival (18–20), we analyzed mitochondrial transcriptional signatures and found a dramatically diminished expression of genes involved in different phases of mitochondrial function in the cycling memory CD4⁺ T cells of INRs (P < 0.05) (Supplemental Figure 5 and Figure 5A). Genes downregulated in cycling memory cells in INRs included COX8, COX5, COX6, and SURF1, which are known components of the mitochondrial respiratory chain; CPTA1 as well as PDK4, genes upstream of fatty acid oxidation (FAO); and IDH1 and IDH2, two enzymes that are critical for glucose-dependent energy production. We found that genes of the NADH family were also expressed at significantly lower levels in the INRs (P < 0.05).

To examine at the single-cell level the mitochondrial defects suggested by transcriptional profiling, we used MitoTracker Green (MG) and MitoTracker Orange (MO) dyes, which quantify mitochondrial mass and OXPHOS, respectively (see Methods). OXPHOS activity, measured by the mean fluorescence intensity (MFI) of MO, was significantly lower (P < 0.05) in cycling CD4⁺

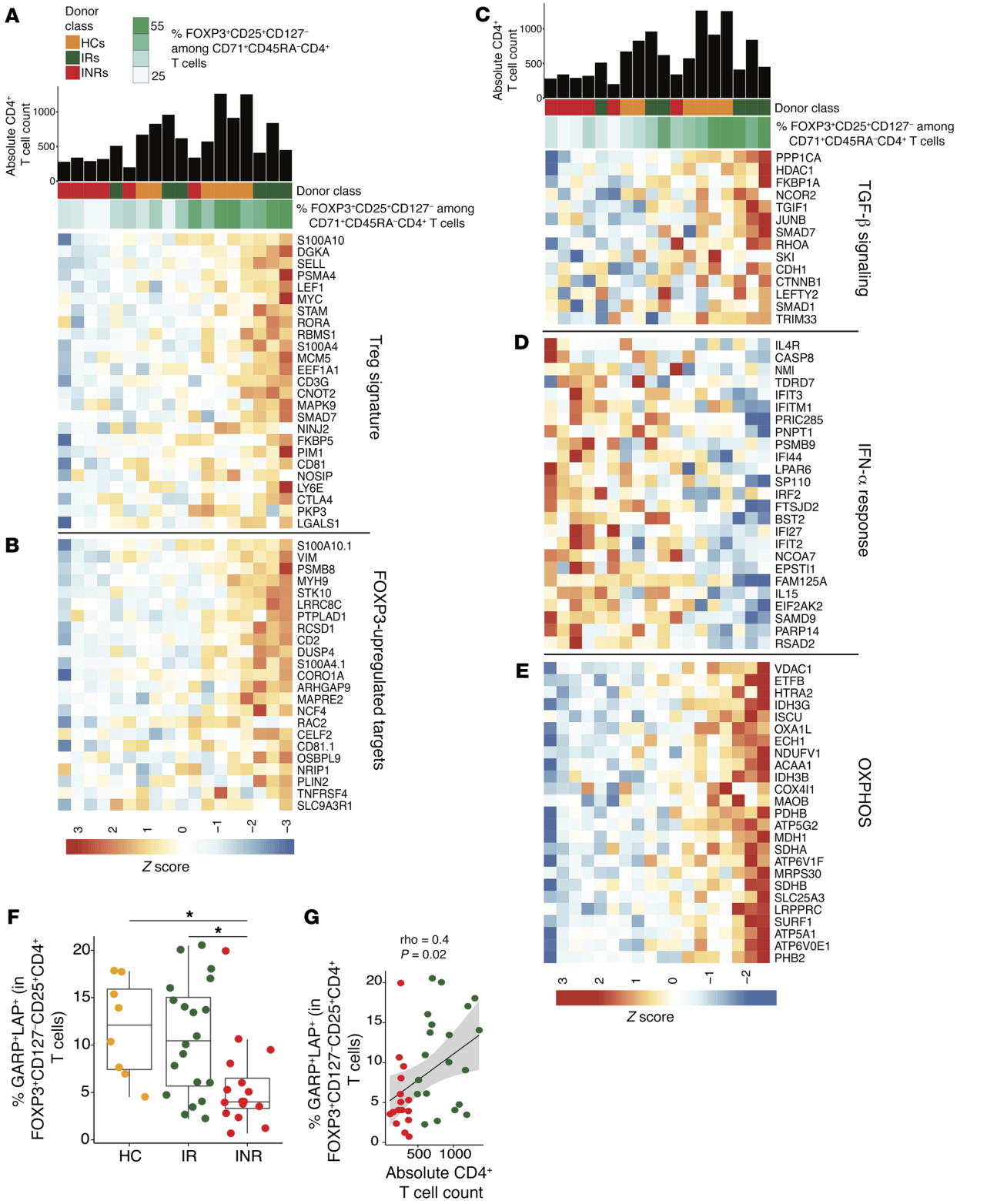

Figure 3. INR Tregs are dysfunctional. Heatmaps showing the expression of Treg signature genes (**A**), FOXP3 upregulated genes (**B**), TGF-β signaling genes (**C**), IFN-α response genes (**D**), and OXPHOS genes (**E**) in cycling memory CD4+ T cells from the 3 donor groups of the Russian cohort. Treg frequency, as defined by FOXP3+CD25+CD127− cells among cycling memory (CD71+CD45RA−CD4+) T cells, is shown as a continuous variable (green gradient). Samples were ordered according to the increasing expression of genes associated with the outcome (mean-rank ordering). Mean-centered gene expression is represented with rows as genes and columns as samples. The bar plot above the heatmap represents absolute CD4+ T cell counts for the subjects. (**F**) Proportion of GARP- and LAP-expressing cells among FOXP3+CD127−CD25+CD45RA−CD4+ T cells from HCs (n = 9), IRs (n = 20), and INRs (n = 16) of the Cleveland cohort. P values were determined by Wilcoxon rank-sum test (*P < 0.05). Data represent the mean ± SD. (**G**) Spearman's correlation between the proportion of GARP+LAP+ cells among Tregs versus the absolute CD4+ T cell count in IRs (n = 20) and INRs (n = 16) of the Cleveland cohort.

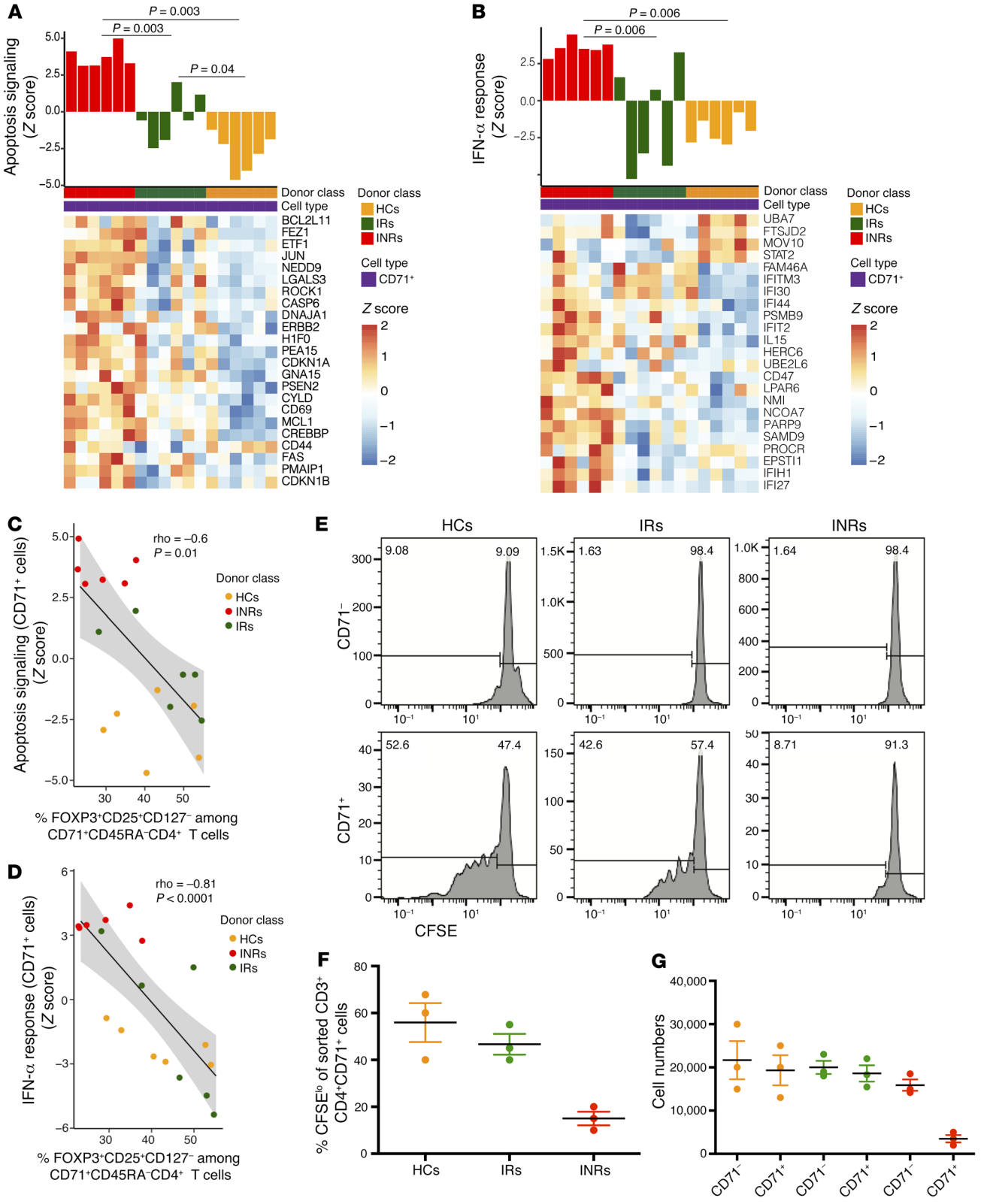
A
P = 0.003
P = 0.003
P = 0.04
Apoptosis signaling (Z score)
Donor class
Cell type
BCL2L11
FEZ1
ETF1
JUN
NEDD9
LGALS3
ROCK1
CASP6
DNAJA1
ERBB2
H1F0
PEA15
CDKN1A
GNA15
PSEN2
CYLD
CD69
MCL1
CREBBP
CD44
FAS
PMAIP1
CDKN1B
Donor class
HCs
IRs
INRs
Cell type
CD71+
Z score
B
P = 0.006
P = 0.006
IFN-α response (Z score)
UBA7
FTSJD2
MOV10
STAT2
FAM46A
IFITM3
IFI30
IFI44
PSMB9
IFIT2
IL15
HERC6
UBE2L6
CD47
LPAR6
NMI
NCOA7
PARP9
SAMD9
PROCR
EPSTI1
IFIH1
IFI27
C
rho = –0.6
P = 0.01
Apoptosis signaling (CD71+ cells) (Z score)
% FOXP3+CD25+CD127– among CD71+CD45RA–CD4+ T cells
D
rho = –0.81
P < 0.0001
IFN-α response (CD71+ cells) (Z score)
% FOXP3+CD25+CD127– among CD71+CD45RA–CD4+ T cells
E
HCs
IRs
INRs
CD71–
CD71+
9.08
9.09
1.63
98.4
1.64
98.4
52.6
47.4
42.6
57.4
8.71
91.3
CFSE
F
% CFSElo of sorted CD3+ CD4+CD71+ cells
HCs
IRs
INRs
G
Cell numbers
CD71–
CD71+
CD71–
CD71+
CD71–
CD71+

Figure 4. Cycling memory CD4⁺ T cells in INRs show increased type I IFN and apoptosis signaling that correlates with low Treg frequencies and is linked to failure to complete the cell cycle and divide. Heatmaps of (**A**) the apoptosis signaling pathway and (**B**) the IFN-α response in cycling memory cells from HCs (n = 6), IRs (n = 6), and INRs (n = 6) of the Russian cohort, identified by the gap statistic (see Methods). The rows represent genes and the columns represent samples. The bar plot above the heatmaps shows the Z score of the pathway in each sample (determined by SLEA; see Methods). P values among SLEA Z scores of the donor groups were determined by a Wilcoxon rank-sum test. (**C**) Spearman's correlations between expression of apoptosis signaling pathway genes (y axis) and (**D**) IFN-α response pathway genes (y axis), with the frequency of Tregs among cycling memory CD4⁺ T cells (x axes) from the Russian cohort subjects. (**E**) Representative histograms showing cell proliferation, measured by the dilution of CFSE dye, of sorted cycling ($CD4^+CD45RA^-CD71^+$) and noncycling ($CD4^+CD45RA^-CD71^-$) memory CD4⁺ T cells after a 7-day in vitro incubation. (**F**) Mean (± SD) percentage of sorted cycling and noncycling memory CD4⁺ T cells that divided at least once after a 7-day in vitro incubation of cells from HCs (n = 3), IRs (n = 3), and INRs (n = 3). (**G**) Mean (± SD) cell count after a 7-day in vitro culture of sorted cycling and noncycling memory CD4⁺ T cells from the same subjects as in **F**. Data in **E**–**G** were derived from Cleveland cohort subjects.

T cells from INR subjects (Figure 5B). This could not be attributed to differences in mitochondrial mass in cycling CD4⁺ T cells from HC, IR, or INR subjects (Figure 5C), as MG fluorescence was similar in the cycling cells from subjects of all groups analyzed. This analysis supported the transcriptional profiling analysis of cycling memory CD4⁺ T cells displayed in Supplemental Figure 5 and Figure 5A. When the mitochondrial analysis was restricted to cycling Tregs, the MFI of both MO and MG was significantly ($P < 0.05$) diminished in the INR subjects (Figure 5, D and E, and Supplemental Figure 6). This was specific to cycling Tregs, as we detected no differences in OXPHOS or mitochondrial mass among the subject groups in $CD71^-$ Tregs or in $CD71^+$ or $CD71^-CD4^+$ T cells that were not Tregs (Supplemental Figure 7).

PGC1α and TFAM expression is diminished in the cycling Tregs of INRs. We next evaluated by flow cytometry the expression of PGC1α, the master regulator of mitochondrial biogenesis (21, 22), and TFAM, a regulator of expression of 13 mitochondrial genes implicated in OXPHOS (37). As shown, cycling Tregs from INRs showed significantly diminished expression of both PGC1α (Figure 5, F and G) and TFAM (Figure 5, F and H), consistent with the decreased mitochondrial mass and decreased OXPHOS in these cells.

IL-15 restores the expression of PGC1α and TFAM in cycling Tregs of INRs. We then asked whether IL-15, a cytokine known to induce OXPHOS and fatty acid β-oxidation in memory CD8⁺ T cells (18, 19), could help restore mitochondrial fitness in the cycling Tregs of INRs. We incubated peripheral blood mononuclear cells (PBMCs) from INR subjects with IL-2 or IL-15 and evaluated PGC1α and TFAM expression in a 20-hour assay. As shown in Figure 5, I and J, IL-15, but not IL-2, significantly induced the expression of PGC1α and TFAM in cycling effector Tregs of INRs. Furthermore, both MG and MO fluorescence significantly increased when sorted Tregs ($CD4^+CD127^-CD25^+$) from INRs were incubated for 7 days with IL-15 (Figure 6, A and B). Sorted Tregs incubated with IL-15 diluted CFSE dye, reflecting successful proliferation in the presence of IL-15 (Figure 6C). In contrast, as shown in Figure 6, IL-2 had no effect on MG or MO fluorescence or the proliferation of INR Tregs. These data suggest that the mitochondrial dysfunction of cycling Tregs from INRs could be improved by IL-15 and that this was associated with induction of PGC1α and TFAM.

Discussion

Earlier work has found high frequencies of cycling among memory CD4⁺ T cells in HIV-infected subjects (38–40). Effective combination antiretroviral therapy leads to a significant decrease in the numbers of cycling cells (1, 41), however, among INRs, despite virologic control, memory CD4⁺ T cell cycling remains elevated. It is not clear whether this increased CD4⁺ T cell memory cycling is a homeostatic consequence of lymphopenia or a driver of CD4 lymphopenia by increasing T cell turnover and cell death. Thus, it is important to define the characteristics of cycling memory CD4⁺ T cells in INR subjects to ascertain whether this increased cycling reflects a "healthy" homeostatic response, or whether it is reflective of a pathophysiologic perturbation that contributes to immune dysregulation.

We show here that cycling memory CD4⁺ T cells obtained from INRs are incapable of completing the cell cycle and proliferating when incubated in culture medium ex vivo. Our ability to sort cycling cells on the basis of surface CD71 expression allowed us to study these cells in isolation and also allowed us to characterize their transcriptional profile. We found that in health and in HIV infection, cycling CD4⁺ T cells were enriched for Tregs as defined by both the transcriptional signature and phenotype.

We report lower frequencies of CD4⁺ T cells with a Treg phenotype in cycling memory CD4⁺ T cells in 2 independent INR cohorts, suggesting that these regulatory cells are not adequately sustained. (Figures 1–3). Tregs proliferate at higher rates than do conventional CD4⁺ T cells in mice (42–44) and humans (45, 46). In humans, Tregs are maintained by a sustained proliferation, as demonstrated by deuterium uptake in vivo (45). The importance of Treg maintenance by proliferation was shown by Carbone et al. (25), who found an impaired capacity of Tregs to proliferate in relapsing-remitting multiple sclerosis and linked diminished Treg expansion to increasing disease severity.

Whether circulating Tregs reflect the function of mucosal Tregs is still unclear. We have discussed elsewhere (47) and provide evidence here that the proinflammatory environment in INR individuals is linked to low numbers of circulating Tregs and functional dysregulation of those that remain. Earlier studies have reported low frequencies of Tregs in the gut mucosa (48) and lymphoid tissues (49) in INR subjects. Yet, from none of those findings can we determine the directionality of these relationships. Our new observations suggest that the maintenance of circulating Tregs is sustained by their ongoing proliferation, gene expression, and metabolic activity, which are linked to CD4⁺ T cell homeostasis. These indices also may be a more accurate reflection of Treg function than is the simple enumeration of Treg phenotype frequencies. Both the numbers and function of Tregs are diminished in the circulation of INRs, but the function of mucosal Tregs in this setting has not yet been studied.

Altogether, our data suggest that the diminished numbers and functional alterations of cycling Tregs are associated with a failure of CD4⁺ T cell recovery and an overall increase in CD4⁺ cell cycling but an impaired ability of these cycling cells to complete the cell cycle and divide in treated HIV-1 infection.

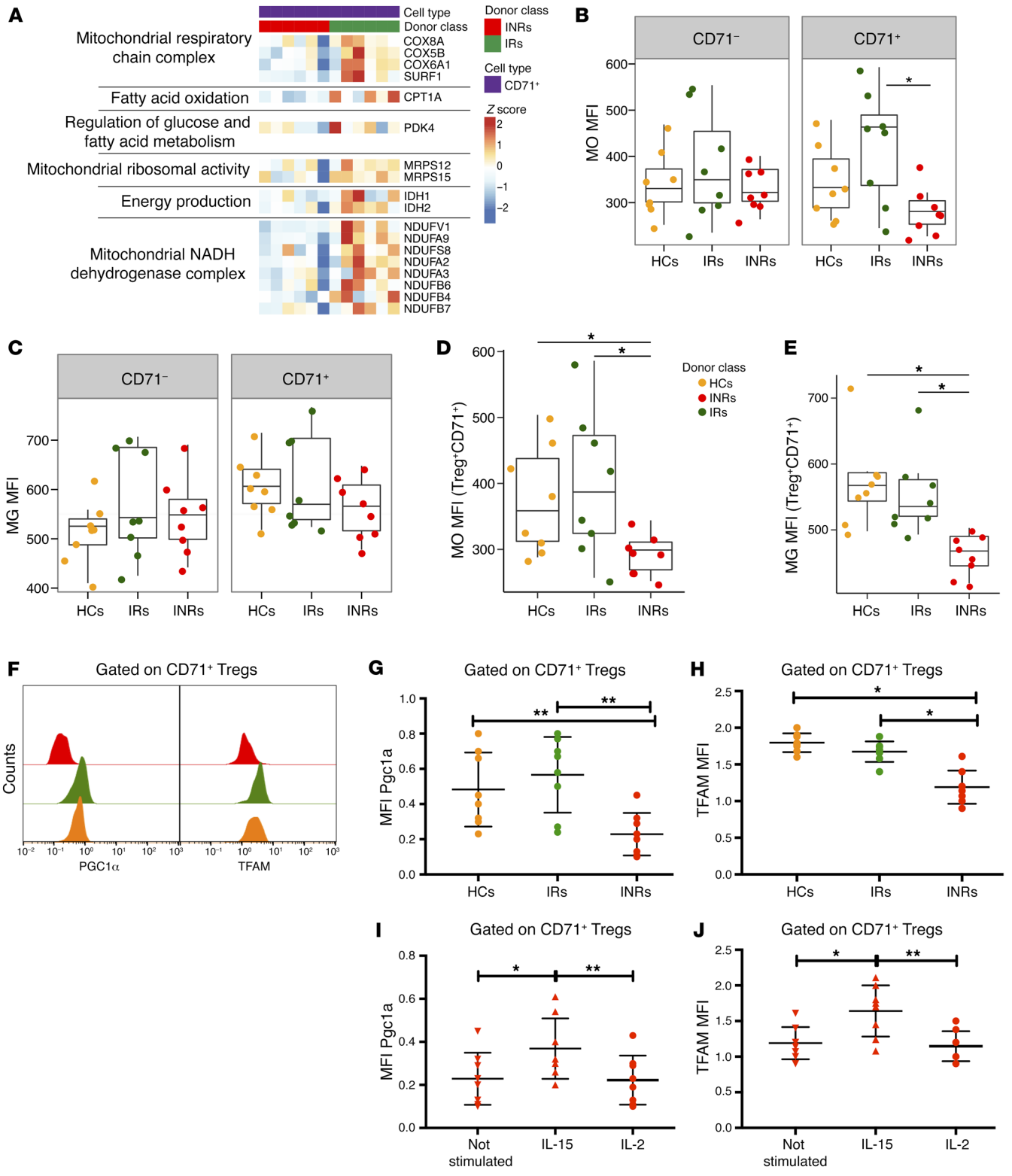

Figure 5. Diminished mitochondrial mass and OXPHOS in cycling Tregs of INRs. (**A**) Heatmap of the OXPHOS pathway showing significant ($P < 0.05$) downregulation in the cycling memory cells of INRs ($n = 6$) compared with those of IRs ($n = 6$) (Russian cohort subjects). The rows represent genes and the columns represent samples. (**B**) OXPHOS estimated by MO fluorescence and (**C**) mitochondrial mass as estimated by MG fluorescence in $CD4^+$C-$D45RA^-CD71^+$ and $CD71^-$ cells from HCs ($n = 8$; orange), IRs ($n = 8$; green), and INRs ($n = 8$; red) (Cleveland cohort subjects). (**D**) OXPHOS and (**E**) mitochondrial mass estimated as above in cycling $CD71^+$ Tregs from HCs, IRs, and INRs. (**F**) Representative histograms of PGC1α and TFAM expression in cycling ($CD71^+$) Tregs from a HC (orange), an IR (green), and an INR (red) subject. Summary MFI of (**G**) PGC1α and (**H**) TFAM expression in cycling ($CD71^+$) Tregs from HCs ($n = 8$), IRs ($n = 8$), and INRs ($n = 8$). Induction of (**I**) PGC1α and (**J**) TFAM following the incubation of PBMCs from INRs ($n = 8$) in medium or medium supplemented with IL-15 (100 ng/ml) or IL-2 (100 ng/ml). $^*P < 0.05$ and $^{**}P < 0.005$, by Wilcoxon rank-sum test. Data shown in **B**–**J** are from the Cleveland cohort subjects and represent the mean ± SD.

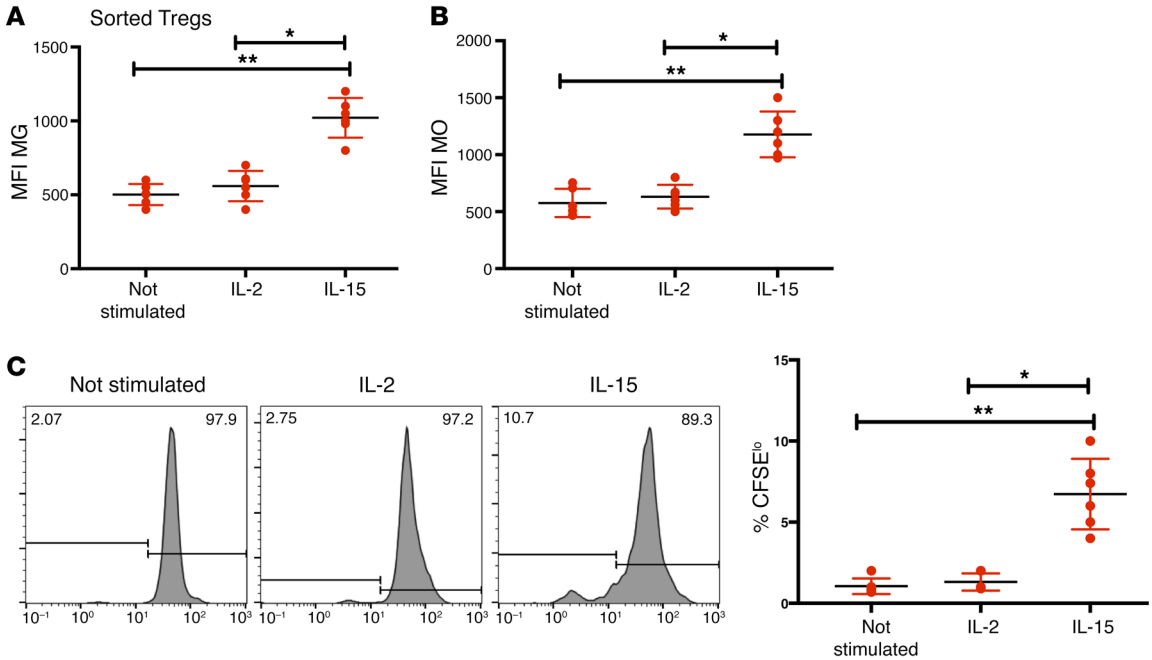

Figure 6. IL-15 restores mitochondrial dysfunction in INR Tregs. Estimation of mitochondrial mass (**A**) and OXPHOS (**B**) by MG and MO MFI on sorted Tregs ($CD127^-CD25^+$) from INRs ($n = 6$) of the Cleveland cohort. (**C**) Cells were left unstimulated or cultured with IL-2 (100 ng/ml) or IL-15 (100 ng/ml) for 7 days and evaluated for proliferation by CFSE dye dilution. $^*P < 0.05$ and $^{**}P < 0.005$, by Wilcoxon rank-sum test. Data represent the mean ± SD.

We suspect that the increased $CD4^+$ T cell cycling seen in INRs represents both a failed homeostatic response as well as a dysregulated control of cellular activation. Our data analysis has led us to build an integrative model (see Methods) that associates the low $CD4^+$ T cell numbers with the interaction between metabolic pathways identified by gene expression and the maintenance of Tregs. The OXPHOS pathway, Treg signature, FOXP3-upregulated targets, and TGF-β signaling are all positively associated with the maintenance of cycling Tregs, which correlated to high $CD4^+$ T cell numbers, while greater apoptosis and type I IFN signatures correlated to low $CD4^+$ T cell numbers (Figure 7 and Supplemental Table 7).

It is interesting that IL-15 mRNA levels were increased in the transcriptional profile of INR cycling $CD4^+$ T cells (Figure 3D), in which exogenous IL-15 could repair the mitochondrial defect observed. And though we have previously reported increased levels of IL-15 in lymphoid tissues of untreated HIV-infected individuals (23), $CD4^+$ T cells are not thought to be important sources of IL-15. The significance of this observation is thus uncertain and should be explored.

IL-15 has been shown to induce the expression of carnitine palmitoyl transferase (CPT1A), a metabolic enzyme that controls the rate-limiting step to mitochondrial FAO and improves mitochondrial OXPHOS in mouse $CD8^+$ T cells (18). Our data are consistent with these findings, as we show that IL-15 induced the expression of PGC1α, the master regulator of many genes implicated in mitochondrial metabolism. PGC1α induces mitochondrial biogenesis in exhausted $CD8^+$ T cells in murine viral infection (22) and murine cancer (21) models, leading to better $CD8^+$ T cell function. Our data extend these findings to human systems, as we showed that the induction of PGC1α and TFAM by IL-15 was associated with increases in mitochondrial mass and OXPHOS of Tregs in HIV-1–infected INR subjects and allowed dysfunctional cycling $CD4^+$ T cells in INRs to complete the cell cycle and divide. These findings suggest that administration of IL-15, a cytokine in human trials for the treatment of cancer (50, 51), could rescue functionally impaired Tregs, which bear features of an exhausted phenotype (52) in INR patients and enhance immune restoration in these subjects.

Methods

Study cohorts. Two cohorts of HIV-1–infected subjects were studied: a Perm, Russia, cohort (Supplemental Table 1) and a Cleveland, Ohio, USA, cohort (Supplemental Table 3).

The Russian cohort consisted of 20 healthy, HIV-uninfected controls (HCs) ($n = 12$ females and 8 males); 21 HIV-1–infected IRs ($n = 17$ females, 4 males); and 16 INRs ($n = 12$ females, 4 males). INR subjects were defined as having $CD4^+$ T cell counts below 350 cells/μl and IRs as having $CD4^+$ T cell counts above 350/μl after at least 2 years of cART with virologic control. The median ages of the HCs, IRs, and INRs were 32, 37, and 35 years, respectively. The HC, IR, and INR groups had median $CD4^+$ T cell counts of 1,071, 582, and 263 cells/μl, respectively. The median duration of cART was 4 years in both IR and INR groups. The Russian cohort's characteristics are detailed in Supplemental Table 1. Listed in Supplemental Table 2 are the subjects for whom microarray transcriptomic analysis was performed. These subjects were selected from the Russian cohort on the basis of sample availability. Gene array analysis was performed on sorted $CD3^+CD4^+CD45RA^-CD71^-$ or $CD71^+$ cells from HCs ($n = 6$), IRs ($n = 6$), and INRs ($n = 6$).

For the Cleveland cohort, 10 HCs ($n = 10$ females), 20 IRs ($n = 14$ males and 6 females), and 16 INRs ($n = 13$ males and 3 females) were recruited with pre-enrollment $CD4^+$ T cell counts below 350/μl for the INRs and above 500/μl for the IRs. The median age was 46, 50, and

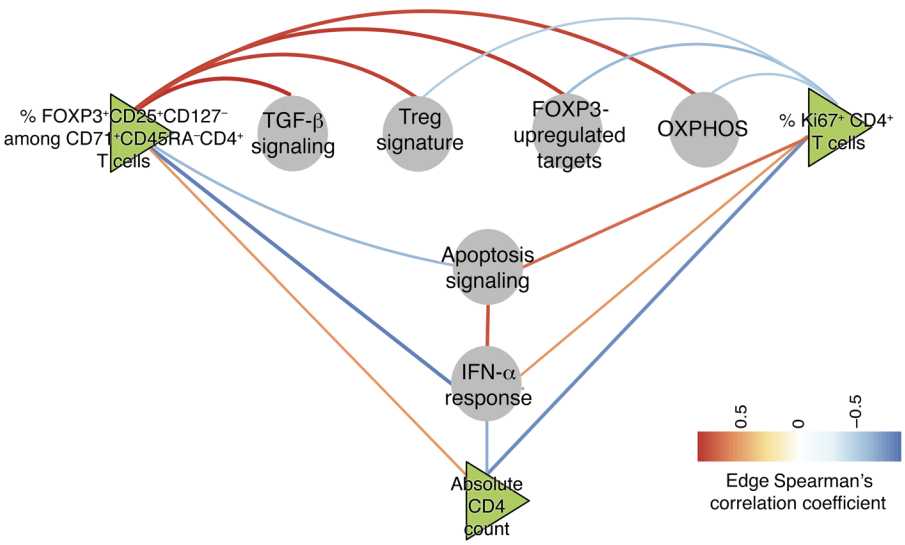

Figure 7. Integrative model showing the correlation between pathway expression and cell phenotypes determined by SLEA. The circle nodes represent the pathway, and the triangle nodes represent the measured markers. The blue lines represent negative Spearman's correlations between nodes, while the red lines represent positive Spearman's correlations ($P < 0.05$). The correlation coefficients (rho) and *P* values are shown in Supplemental Table 7.

51 years for the HCs, IRs, and INRs, respectively. The median $CD4^+$ T cell count was 887 and 277 for the IRs and INRs, respectively. The median duration of cART treatment was 8 years and 8.8 years for the IRs and INRs, respectively. The Cleveland cohort's characteristics are described in Supplemental Table 3.

Microarray. For microarray analysis, cryopreserved PBMCs from the Russian cohort of 6 HCs, 6 INRs, and 6 IRs (Supplemental Table 2) were thawed and stained with anti-CD3, anti-CD4, anti-CD45RA, and anti-CD71 antibodies. Twenty thousand $CD3^+CD4^+CD45RA^+CD71^+$ and $CD71^-$ cells were sorted into RLT lysis buffer (catalog 79216, QIAGEN). RNA was isolated and biotinylated (catalog 338904, QIAGEN), and complementary RNA (cRNA) was hybridized to the Illumina HT-12V4 expression bead chips and quantified using Illumina Genome Studio software. The data have been deposited in the NCBI's Gene Expression Omnibus (GEO) database (GEO GSE106792).

Flow cytometry. To analyze cycling and noncycling $CD4^+$ T cells and Treg phenotypes by flow cytometry, fluorochrome-conjugated monoclonal antibodies targeting the following human antigens were used: CD25 BUV395 (clone 2A3, catalog 564034, BD); CD127 BV786 (clone HIL-7R-M21, catalog 563324, BD Biosciences); CD45RA BV650 (clone H100, catalog 304136, BioLegend); CD4-QDOT605 (clone S3.5, catalog Q10008, Thermo Fisher Scientific); GARP PECY7 (clone 7B11, catalog 352508, BioLegend); LAP PE-CF594 (clone TW4-2F8, catalog 562490, BD Biosciences); CD3 BUV737 (clone UCHT1, catalog 564307, BD Biosciences); FOXP3 PE (clone 236/E7, catalog 12-4777-42, eBioscience); PGC1α-DyLight 488 (catalog NBP1-04676G, Novus Biologicals); and TFAM Alexa Fluor 488 (catalog ab198308, Abcam). The intracellular detection of PGC1α and TFAM was evaluated using the Transcription Factor Kit (catalog 72-5774-40, eBioscience, Thermo Fisher Scientific) according to the manufacturer's protocol. Living cells were identified using a LIVE/DEAD Fixable Aqua Dead Cell Stain Kit (catalog L34957, Invitrogen, Thermo Fisher Scientific). Between 1 and 2 million PBMCs were examined by flow cytometry (Fortessa, BD Biosciences) and analyzed using Flowjo software (Tree Star). For cell-sorting and cell proliferation assessment, the anti-CD71 clone b3/25 was used (catalog sc-65877, Santa Cruz Biotechnology) and locally conjugated to RPE (catalog LNK022RPE, AbD Serotec) according to the manufacturer's protocol. Treg sorting was performed using a Regulatory T Cell Isolation Kit II (130-094-775, Miltenyi Biotec).

MG (M-7514) and MO (M-7511) were obtained from Life Technologies (Thermo Fisher Scientific) and used according to the manufacturer's protocol. MG is nonfluorescent in aqueous solution and becomes fluorescent only when it accumulates in the mitochondrial lipid environment, regardless of membrane potential. MO is a nonfluorescent dye that, upon oxidation, becomes fluorescent, allowing mitochondrial OXPHOS estimation.

Statistical analysis of flow cytometric data. Wilcoxon rank-sum tests were used to determine statistical differences in pairwise comparisons. The *P* values were then adjusted for multiple comparisons using the Benjamini and Hochberg (BH) method.

Transcriptional profiling of microarray data. Analysis of the raw quantified microarray output data was conducted using Bioconductor R software. Missing gene expression data were imputed using nearest-neighbor averaging (https://bioconductor.org/packages/release/bioc/html/impute.html). Gene expression was quantile normalized and then $\log_2$ transformed to reduce variability. Sample outliers based on gene expression were detected and removed. Hierarchical clustering methods and multidimensional scaling analysis were used to evaluate similarities or differences in gene expression profiles between samples.

To detect differences in gene expression between groups of interest, the LIMMA package (53) was used to fit a linear regression model to each probe, with transcript expression as the dependent variable and the group of interest as the independent variable. For each model, a moderated *t* test was used to test whether the fold changes were different from zero. The *P* values were then adjusted for multiple comparisons using the BH method (54). To identify pathways enriched for the genes differentially expressed among the groups compared, gene set enrichment analysis (GSEA) (55) preranked by the decreasing order of the *t* statistic of the genes was performed. The Hallmark gene sets from the Molecular Signatures Database (MSigDB), along with a Treg signature (56) and target genes of FOXP3 (26), were used as the pathway database. The *P* values of the enriched pathways were then adjusted using the BH method, and pathways with *P* values of less than 5% were reported.

To identify modules of cell-cycling pathways among the genes differentially expressed between cycling and noncycling memory cells in

each subject group, we grouped pathways into modules on the basis of at least 25% gene overlap (Jaccard index) between pathways using the enrichment map strategy (57). The most frequent genes among the pathways in a module, defined as genes that were enriched in at least 50% of the pathways in each module, were represented.

Association of gene expression with outcome. We determined the association of gene expression with the measured outcome (percentage of $FOXP3^+CD25^+CD127^-$ cells among $CD71^+CD45RA^-CD4^+$ T cells) by fitting a linear regression model with the transcript expression as a dependent variable and the outcome as an independent variable. The outcome was kept as a continuous variable. A moderated *t* test was performed to determine whether the coefficient of regression of each transcript was different from zero, and the obtained *P* values were adjusted for multiple comparisons using the BH method.

To identify pathways among the genes associated with the outcomes, GSEA with 1,000 permutations was performed on genes preranked by the decreasing order of their *t* statistic using the Hallmark gene sets of MSigDB (55). The *P* values of the enriched pathways were adjusted by the BH method, and pathways with *P* values of less than 5% were reported.

For the integrative model, a correlation between pathways and the outcomes was determined by sample-level enrichment analysis (SLEA) by calculating the *Z* score of each pathway per sample (58). The mean expression value of genes of a selected pathway was compared with the mean expression of 1,000 random gene sets of the same size of the selected pathway for every sample. The difference between the observed and expected mean expression values for each gene set was calculated.

Gap statistic approach. We identified transcripts that were significantly ($P < 0.05$) differentially expressed among the 3 donor classes in the cycling cell population. Hierarchical clustering of these genes revealed 2 major clusters in which the gene expression profiles of the HCs and IRs were similar and distinct from those of the INRs. Clusters of genes that showed unique/distinct gene expression profiles in the 3 classes of subjects were identified using the gap statistic strategy (35). Pathways (Hallmark gene sets from the MSigDB) specific to each cluster of genes were then identified using a Fisher's exact test. The *P* values of pathways were then adjusted for multiple comparisons using the BH method.

Study approval. This study was approved by the IRBs of the University Hospitals Case Medical Center and the Perm Regional Center for Protection against AIDS and Infectious Diseases (Perm, Russia). Written informed consent was obtained from all subjects.

Author contributions

SAY designed, performed, and analyzed experiments and, together with AT, SPR, and MML, wrote the manuscript. AT performed all gene array and statistical analyses. SPR developed and ran all the flow panels to validate the gene signatures, including the MitoTrackers and flow cytometry–based multicolor assays. SPR and SAY analyzed the panels. EVS and LBK also performed flow cytometric analyses. CLS, SP, and SZ performed experiments. KVS, MLF, and BR provided patients' PBMCs. MC generated gene array data. RB provided conjugated antibodies. MML, LM, DCD, DDA, PP, SFS, and LHC participated in the overall design of the study. All authors contributed to the discussion of the project and reviewed and approved the manuscript.

Acknowledgments

This work was supported by grants from the NIAID (AI 105937 and AI 68636); the National Institutes of Drug Abuse (DA044135); the Fasenmyer Foundation; the Case Western Reserve University Center for AIDS Research (CFAR) (AI-036219); the Russian Foundation for Basic Research (17-54-30006); and by a VA Merit Award (CX001104-04).

Address correspondence to: Michael M. Lederman or Souheil-Antoine Younes, Division of Infection Diseases, Case Western Reserve University, 2109 Adelbert Road, BRB 1048, Cleveland, Ohio 44106, USA. Phone: 216.368.4853; Email: lederman.michael@clevelandactu.org (MML). Phone: 216.368.1705; Email: Sxy292@case.edu (SAY).

1. Lederman MM, et al. Immunologic failure despite suppressive antiretroviral therapy is related to activation and turnover of memory CD4 cells. *J Infect Dis*. 2011;204(8):1217–1226.
2. Piconi S, et al. Immune activation, apoptosis, and Treg activity are associated with persistently reduced $CD4^+$ T-cell counts during antiretroviral therapy. *AIDS*. 2010;24(13):1991–2000.
3. Baker JV, et al. CD4+ count and risk of non-AIDS diseases following initial treatment for HIV infection. *AIDS*. 2008;22(7):841–848.
4. Lewden C, et al. HIV-infected adults with a CD4 cell count greater than 500 cells/mm3 on long-term combination antiretroviral therapy reach same mortality rates as the general population. *J Acquir Immune Defic Syndr*. 2007;46(1):72–77.
5. Min B, Paul WE. Endogenous proliferation: burst-like CD4 T cell proliferation in lymphopenic settings. *Semin Immunol*. 2005;17(3):201–207.
6. Kelley CF, et al. Incomplete peripheral $CD4^+$ cell count restoration in HIV-infected patients receiving long-term antiretroviral treatment. *Clin Infect Dis*. 2009;48(6):787–794.
7. Robbins GK, et al. Incomplete reconstitution of T cell subsets on combination antiretroviral therapy in the AIDS Clinical Trials Group protocol 384. *Clin Infect Dis*. 2009;48(3):350–361.
8. Shive CL, et al. Inflammatory cytokines drive CD4+ T-cell cycling and impaired responsiveness to interleukin 7: implications for immune failure in HIV disease. *J Infect Dis*. 2014;210(4):619–629.
9. Shive CL, et al. Inflammation perturbs the IL-7 axis, promoting senescence and exhaustion that broadly characterize immune failure in treated HIV infection. *J Acquir Immune Defic Syndr*. 2016;71(5):483–492.
10. Marziali M, et al. T-cell homeostasis alteration in HIV-1 infected subjects with low CD4 T-cell count despite undetectable virus load during HAART. *AIDS*. 2006;20(16):2033–2041.
11. Nguyen TP, et al. Responsiveness to IL-7 but not to IFN-α is diminished in $CD4^+$ T cells from treated HIV infected patients who experience poor $CD4^+$ T-cell recovery. *AIDS*. 2016;30(13):2033–2042.
12. Kaufmann GR, et al. Characteristics, determinants, and clinical relevance of CD4 T cell recovery to < 500 cells/microL in HIV type 1-infected individuals receiving potent antiretroviral therapy. *Clin Infect Dis*. 2005;41(3):361–372.
13. Engsig FN, et al. Long-term mortality in HIV patients virally suppressed for more than three years with incomplete CD4 recovery: a cohort study. *BMC Infect Dis*. 2010;10:318.
14. D'Amico R, et al. Lower $CD4^+$ T lymphocyte nadirs may indicate limited immune reconstitution in HIV-1 infected individuals on potent antiretroviral therapy: analysis of immunophenotypic marker results of AACTG 5067. *J Clin Immunol*. 2005;25(2):106–115.
15. Moore RD, Keruly JC. $CD4^+$ cell count 6 years after commencement of highly active antiretroviral therapy in persons with sustained virologic suppression. *Clin Infect Dis*. 2007;44(3):441–446.
16. Greub G, et al. Clinical progression, survival, and immune recovery during antiretroviral therapy in patients with HIV-1 and hepatitis C virus coinfection: the Swiss HIV Cohort Study. *Lancet*. 2000;356(9244):1800–1805.
17. Shmagel KV, et al. Influence of hepatitis C

virus coinfection on CD4+ T cells of HIV-infected patients receiving HAART. *AIDS*. 2014;28(16):2381–2388.
18. van der Windt GJ, et al. Mitochondrial respiratory capacity is a critical regulator of CD8+ T cell memory development. *Immunity*. 2012;36(1):68–78.
19. Buck MD, et al. Mitochondrial dynamics controls T cell fate through metabolic programming. *Cell*. 2016;166(1):63–76.
20. Ron-Harel N, Sharpe AH, Haigis MC. Mitochondrial metabolism in T cell activation and senescence: a mini-review. *Gerontology*. 2015;61(2):131–138.
21. Scharping NE, et al. The tumor microenvironment represses T cell mitochondrial biogenesis to drive intratumoral T cell metabolic insufficiency and dysfunction. *Immunity*. 2016;45(3):701–703.
22. Bengsch B, et al. Bioenergetic insufficiencies due to metabolic alterations regulated by the inhibitory receptor PD-1 are an early driver of CD8(+) T cell exhaustion. *Immunity*. 2016;45(2):358–373.
23. Younes SA, et al. IL-15 promotes activation and expansion of CD8+ T cells in HIV-1 infection. *J Clin Invest*. 2016;126(7):2745–2756.
24. Motamedi M, Xu L, Elahi S. Correlation of transferrin receptor (CD71) with Ki67 expression on stimulated human and mouse T cells: the kinetics of expression of T cell activation markers. *J Immunol Methods*. 2016;437:43–52.
25. Carbone F, et al. Regulatory T cell proliferative potential is impaired in human autoimmune disease. *Nat Med*. 2014;20(1):69–74.
26. Marson A, et al. Foxp3 occupancy and regulation of key target genes during T-cell stimulation. *Nature*. 2007;445(7130):931–935.
27. Yamagiwa S, Gray JD, Hashimoto S, Horwitz DA. A role for TGF-beta in the generation and expansion of CD4+CD25+ regulatory T cells from human peripheral blood. *J Immunol*. 2001;166(12):7282–7289.
28. Bennett CL, et al. The immune dysregulation, polyendocrinopathy, enteropathy, X-linked syndrome (IPEX) is caused by mutations of FOXP3. *Nat Genet*. 2001;27(1):20–21.
29. Brunkow ME, et al. Disruption of a new forkhead/winged-helix protein, scurfin, results in the fatal lymphoproliferative disorder of the scurfy mouse. *Nat Genet*. 2001;27(1):68–73.
30. Hashimoto H, Ueda R, Narumi K, Heike Y, Yoshida T, Aoki K. Type I IFN gene delivery suppresses regulatory T cells within tumors. *Cancer Gene Ther*. 2014;21(12):532–541.
31. Srivastava S, Koch MA, Pepper M, Campbell DJ. Type I interferons directly inhibit regulatory T cells to allow optimal antiviral T cell responses during acute LCMV infection. *J Exp Med*. 2014;211(5):961–974.
32. Tran DQ, Andersson J, Wang R, Ramsey H, Unutmaz D, Shevach EM. GARP (LRRC32) is essential for the surface expression of latent TGF-β on platelets and activated FOXP3+ regulatory T cells. *Proc Natl Acad Sci U S A*. 2009;106(32):13445–13450.
33. Procaccini C, et al. The proteomic landscape of human ex vivo regulatory and conventional T cells reveals specific metabolic requirements. *Immunity*. 2016;44(2):406–421.
34. Beier UH, et al. Essential role of mitochondrial energy metabolism in Foxp3+ T-regulatory cell function and allograft survival. *FASEB J*. 2015;29(6):2315–2326.
35. Tibshirani R, Walther G, Hastie T. Estimating the number of clusters in a data set via the gap statistic. *J Roy Stat Soc B*. 2001;63:411–423.
36. Crouse J, Kalinke U, Oxenius A. Regulation of antiviral T cell responses by type I interferons. *Nat Rev Immunol*. 2015;15(4):231–242.
37. Lin J, Handschin C, Spiegelman BM. Metabolic control through the PGC-1 family of transcription coactivators. *Cell Metab*. 2005;1(6):361–370.
38. Jiang W, et al. Cycling memory CD4+ T cells in HIV disease have a diverse T cell receptor repertoire and a phenotype consistent with bystander activation. *J Virol*. 2014;88(10):5369–5380.
39. Hazenberg MD, et al. T-cell division in human immunodeficiency virus (HIV)-1 infection is mainly due to immune activation: a longitudinal analysis in patients before and during highly active antiretroviral therapy (HAART). *Blood*. 2000;95(1):249–255.
40. Kovacs JA, et al. Identification of dynamically distinct subpopulations of T lymphocytes that are differentially affected by HIV. *J Exp Med*. 2001;194(12):1731–1741.
41. Funderburg NT, et al. Dynamics of immune reconstitution and activation markers in HIV+ treatment-naïve patients treated with raltegravir, tenofovir disoproxil fumarate and emtricitabine. *PLoS One*. 2013;8(12):e83514.
42. Younes SA, Punkosdy G, Caucheteux S, Chen T, Grossman Z, Paul WE. Memory phenotype CD4 T cells undergoing rapid, nonburst-like, cytokine-driven proliferation can be distinguished from antigen-experienced memory cells. *PLoS Biol*. 2011;9(10):e1001171.
43. Fisson S, et al. Continuous activation of autoreactive CD4+ CD25+ regulatory T cells in the steady state. *J Exp Med*. 2003;198(5):737–746.
44. Min B, et al. Gut flora antigens are not important in the maintenance of regulatory T cell heterogeneity and homeostasis. *Eur J Immunol*. 2007;37(7):1916–1923.
45. Vukmanovic-Stejic M, et al. Human CD4+ CD25hi Foxp3+ regulatory T cells are derived by rapid turnover of memory populations in vivo. *J Clin Invest*. 2006;116(9):2423–2433.
46. Booth NJ, et al. Different proliferative potential and migratory characteristics of human CD4+ regulatory T cells that express either CD45RA or CD45RO. *J Immunol*. 2010;184(8):4317–4326.
47. Pandiyan P, et al. Mucosal regulatory T cells and T helper 17 cells in HIV-associated immune activation. *Front Immunol*. 2016;7:228.
48. Rueda CM, Velilla PA, Chougnet CA, Rugeles MT. Incomplete normalization of regulatory t-cell frequency in the gut mucosa of Colombian HIV-infected patients receiving long-term antiretroviral treatment. *PLoS One*. 2013;8(8):e71062.
49. Gaardbo JC, et al. Regulatory T cells in HIV-infected immunological nonresponders are increased in blood but depleted in lymphoid tissue and predict immunological reconstitution. *J Acquir Immune Defic Syndr*. 2014;66(4):349–357.
50. Romee R, et al. First-in-human phase 1 clinical study of the IL-15 superagonist complex ALT-803 to treat relapse after transplantation. *Blood*. 2018;131(23):2515–2527.
51. Ng SSM, et al. Heterodimeric IL15 treatment enhances tumor infiltration, persistence, and effector functions of adoptively transferred tumor-specific T cells in the absence of lymphodepletion. *Clin Cancer Res*. 2017;23(11):2817–2830.
52. Yang K, et al. Homeostatic control of metabolic and functional fitness of Treg cells by LKB1 signalling. *Nature*. 2017;548(7669):602–606.
53. Ritchie ME, et al. limma powers differential expression analyses for RNA-sequencing and microarray studies. *Nucleic Acids Res*. 2015;43(7):e47.
54. Reiner A, Yekutieli D, Benjamini Y. Identifying differentially expressed genes using false discovery rate controlling procedures. *Bioinformatics*. 2003;19(3):368–375.
55. Subramanian A, et al. Gene set enrichment analysis: a knowledge-based approach for interpreting genome-wide expression profiles. *Proc Natl Acad Sci U S A*. 2005;102(43):15545–15550.
56. Pfoertner S, et al. Signatures of human regulatory T cells: an encounter with old friends and new players. *Genome Biol*. 2006;7(7):R54.
57. Merico D, Isserlin R, Stueker O, Emili A, Bader GD. Enrichment map: a network-based method for gene-set enrichment visualization and interpretation. *PLoS One*. 2010;5(11):e13984.
58. Gundem G, Lopez-Bigas N. Sample-level enrichment analysis unravels shared stress phenotypes among multiple cancer types. *Genome Med*. 2012;4(3):28.